Power-Quality Improvement of a Stand-Alone Induction Generator Using a STATCOM With Battery Energy Storage System

J. A. Barrado, R. Griñó, *Member, IEEE*, and H. Valderrama-Blavi, *Member, IEEE*

***Abstract*—This paper presents a STATCOM with a self-oscillating bidirectional dc–dc converter for interfacing battery energy storage in a stand-alone induction generator system. The self-oscillation mode is based on relay feedback control with hysteresis. To reduce the output current ripple, an LCL filter is connected between the half bridge of this dc–dc converter and the energy storage system. The other side of bidirectional converter is coupled with a voltage-source converter. The proposed control allows that the previous electronic converters, with an additional resistive dump load, compensate all disturbances in a self-excited induction generator due to three-phase four-wire loads and an improvement of system efficiency. The simulated results show good performance of the stand-alone power system under different loading conditions.**

***Index Terms*—Battery energy storage (BES) system, relay feedback control, self-excited induction generator (SEIG), self-oscillating bidirectional converter, static compensator (STATCOM).**

I. Introduction

THE ACTUAL consumer society imposes a permanent increase in energy consumption, causing a progressive exhaustion of fossil fuels, the main resources that are used. In addition, the expansion of renewable energy sources is not being developed at the same rate as the growing demand. For these reasons, it is important to encourage energy savings, take steps to increase energy efficiency, boost the use, research and develop renewable energies, and finally protect the natural environment as much as possible.

The advantages of self-excited induction generators (SEIG) have led to them being chosen as suitable candidates for the energy supply in rural communities and remote areas, where these machines can be driven by using diesel engines or some renewable energy resources, such as wind energy or microhydropower.

When a three-phase four-wire SEIG feeds unbalanced and/or nonlinear loads, the terminal voltage and stator currents are also unbalanced and may appear as current and voltage harmonics that increase power losses, create unequal heating, and cause torque pulsation on the shaft of the generator. Besides this, unbalanced three-phase currents yield a current in the neutral wire, causing additional power losses and heating.

To solve these problems, some converter topologies and control architectures have been proposed [1], [2]. In [3], an SEIG-STATCOM system operates in collaboration with a bidirectional dc–dc converter and battery bank. This feature increases the system efficiency and capability. Based on this power system, our contribution proposes some improvement, these are: 1) the STATCOM including a block to compensate the current in the neutral wire of an induction generator and voltage asymmetries on the dc bus of the converter and 2) the battery bank is connected to a self-oscillating dc–dc converter [4] based in a relay feedback control [5]. This choice provides certain advantages over other options of bidirectional dc–dc converters [6], such as simplicity of design, good performance over a wide operating range, robustness, and lower cost. So the proposed bidirectional dc–dc converter is an interesting option to consider in other renewable energy systems, electric vehicles, or satellite applications.

II. System Description

The system under study consists of a stand-alone SEIG, working at constant power conditions and driven by a micro hydro turbine. The generator supplies a three-phase four-wire system containing any kind of load. The voltage and frequency control are achieved by means of an electronic converter connected to the generator terminals with the necessary control loops to regulate these electrical variables (Fig. 1).

The SEIG is a three-phase induction machine, with a squirrel cage rotor and a wye-connected stator winding with its middle point connected to the system's neutral wire. The prime mover drives the rotor at a speed higher than the synchronous one. Finally, a three-phase shunt capacitor bank supplies constant reactive power to the SEIG.

The electronic converter consists of a four-leg voltage-source converter (VSC), with a split-capacitor bus, and two dc–dc converters: a chopper and a battery energy storage (BES) system.

The three-phase four-wire VSC acts as an active filter, static var compensator, as well as a load balancing and ac voltage regulator. The split-capacitor VSC contains a fourth leg to compensate the neutral current (NCC) yielded by the unbalanced ac load system and voltage asymmetries on dc bus capacitors of VSC [7].

Manuscript received April 14, 2009; revised April 28, 2010. Date of publication September 02, 2010; date of current version September 22, 2010. This work was supported by the Spanish "Ministerio de Educación y Ciencia" under Grant DPI2006-15627-CO3/03. Paper no. TPWRD-00219-2009.

J. A. Barrado and H. Valderrama-Blavi are with the Department of Electronic Engineering and Automatic Control, Universitat Rovira i Virgili, Tarragona 43007, Spain (e-mail: joseantonio.barrado@urv.cat, hugo.valderrama@urv.cat).

R. Griñó is with the Institute of Industrial and Control Engineering, Universitat Politècnica de Catalunya; Barcelona 08028, Spain (e-mail: roberto.grino@upc.edu).

Digital Object Identifier 10.1109/TPWRD.2010.2051565

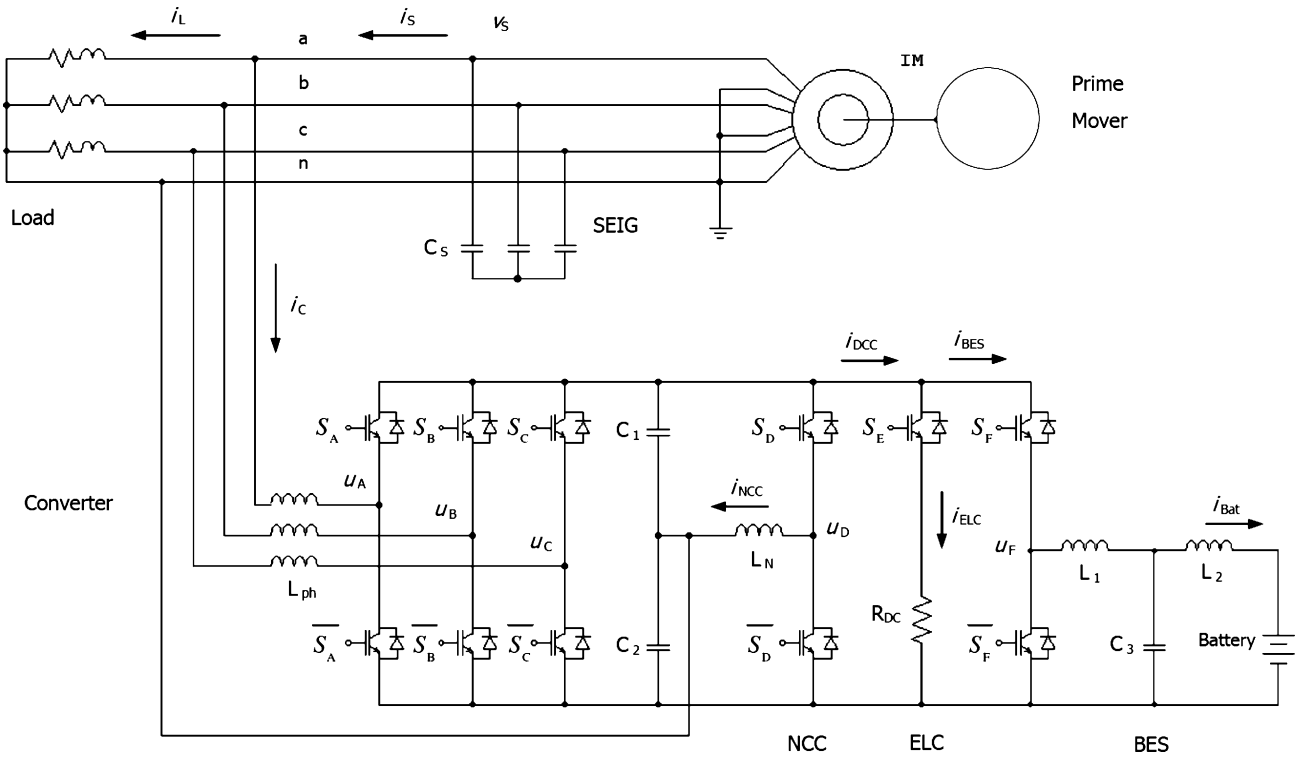

Fig. 1. Schematic diagram of the power system.

The dc–dc converters regulate the frequency at the ac side of system. One of them acts as an electronic load controller (ELC) [8] by means a chopper connected to a resistive load. The two insulated-gate bipolar transistors (IGBTs) of the second dc-dc converter are switched in a complementary form. Its duty cycle determines the battery current (I_{Bat}) direction and magnitude. Since $\mathrm{V_{Bat}} < \mathrm{V_{DC}}$, the bidirectional converter operates in buck or boost mode. It acts as a buck converter in the charging phase of the BES unit and as a boost converter in the discharging phase. Thus, this last converter allows the battery to store/supply energy from/to the ac side of the system.

The voltage pulses of the battery converter are filtered by a third-order LCL filter. The transfer function of this passive filter, defined by the input filter voltage (U_F) and the current-through output inductor $(\mathrm{L_2})$, is shown at (1), at the bottom of the page, where $\mathrm{R_{L1}}$ and $\mathrm{R_{L1}}$ model the losses in the respective inductors $\mathrm{L_1}$ and $\mathrm{L_2}$.

The chosen topology allows higher attenuation of the high-frequency harmonic content in the battery current than the usual L-filter. The LCL filter of battery converter can be designed from [9]. Thus, in the low-frequency region, as the sum of $\mathrm{L_1}$ and $\mathrm{L_2}$ is smaller than the L-filter inductance, the voltage drop across the LCL filter is lower than the L-filter case. As a result, the dc losses are lower, an additional advantage.

The battery bank is composed of 26 identical lead-acid batteries connected in series. To make the analysis easier, the battery model is given by the equivalent battery internal electromotive force (emf) and series resistance [10].

III. Control Strategy

Fig. 2 shows the block diagram of the proposed control architecture. The controller forces the electronic converter to compensate the load current (i_{L}) and to absorb/inject a determinate value of active power from/to the ac system. Thus, the current supply from SEIG (i_{S}) becomes sinusoidal, balanced and the values of voltage and frequency are kept constant.

Therefore, the induction generator provides the active power demanded by the load and the other active power necessary to keep the voltage in the dc bus (v_{DC}) of the converter. This additional component determines a current value to cover the losses in the power converter (switching losses of IGBTs, leakage current of capacitors, etc.), to supply the current of controlled dc load (i_{ELC}) and to charge the battery bank (i_{Bat}).

A. Current Control of Three-Phase Four-Wire VSC

The main block of the proposed control is based on a three-phase phase-locked loop (PLL) structure (Fig. 3). A first block computes the abc to $dq0$ transformation (in the synchronous

$$G(s) = \frac{1}{\mathrm{C_3L_1L_2}s^3 + \mathrm{C_3(L_1R_{L2} + L_2R_{L1})}s^2 + (\mathrm{C_3R_{L1}R_{L2} + L_1 + L_2})s + \mathrm{R_{L1} + R_{L2}}} \quad (1)$$

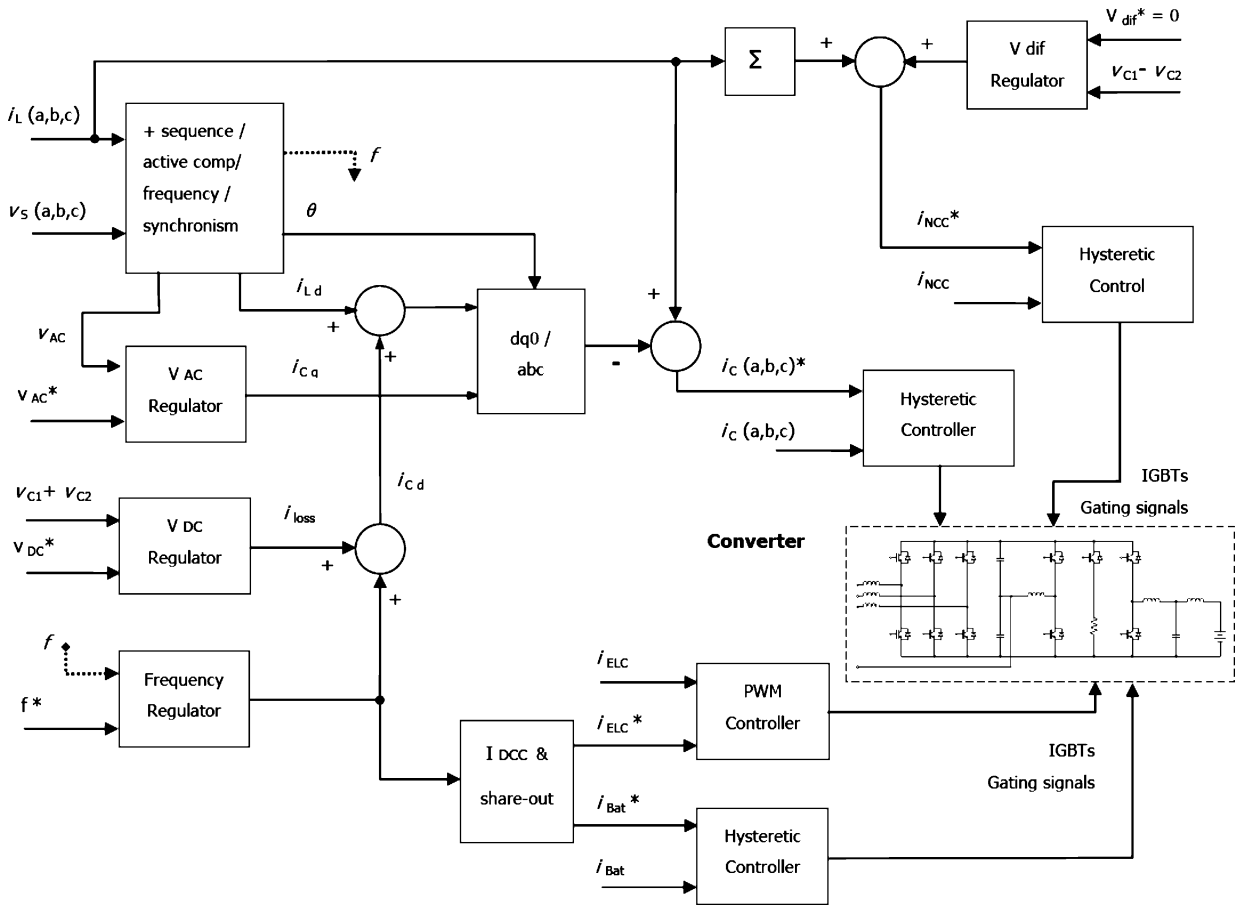

Fig. 2. Block diagram of the power converter controller.

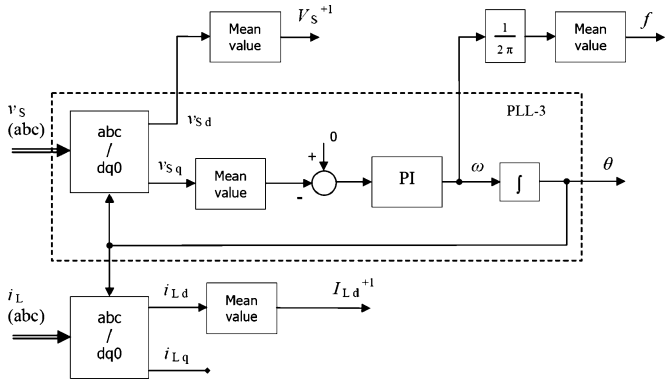

Fig. 3. Determination of the positive-sequence fundamental components through a three-phase PLL.

reference frame) of three-phase voltage signals v_{S} (abc). Other blocks extract the magnitude and the frequency of the positive-sequence fundamental component of voltage line [11]. And, finally, this structure performs the active part of the positive-sequence fundamental component (I_{Ld}^{+1}) of load current i_{L} (abc).

However, when load is unbalanced or/and nonlinear, the i_{Ld} signal presents an oscillatory component (2)

$$i_{\mathrm{Ld}} = \bar{i}_{\mathrm{L\,d}} + \tilde{i}_{\mathrm{L\,d}}. \tag{2}$$

Through a set of mean value blocks, the respective positive-sequence fundamental component $(V_{\mathrm{AC}}^{+1}, I_{Ld}^{+1})$ is extracted from the three-phase voltage system and load current.

Later, a transformation block $dq0$–abc generates the three-phase balanced active component of the load current i_{Ld} (abc). The difference between this generated value and the measured load current i_L (abc) yields the reference current to compensate the reactive power and the unbalanced currents and harmonics of the three-phase load.

The total reference signal of the VSC current controller i_{C} (abc)* is the sum of the aforementioned component (compensated load current) and two other components: the signals i_{Cd} and i_{Cq}.

The reference i_{Cd} is the active current required to balance the active power in the whole system in order to maintain the desired frequency (through a frequency regulator) and to compensate the losses in the electronic converter (by means of a dc voltage regulator). The frequency regulator establishes the three-phase current magnitude, in phase with SEIG voltage signals. The feedback control loop of the dc voltage regulator gives another reference signal i_{loss} to make the converter absorb in-phase fundamental ac current to compensate the aforementioned dc voltage variation [12].

On the other hand, the signal i_{Cq} is a reference current that sets the required reactive power to compensate the ac voltage variations on a stand-alone induction generator. This reactive

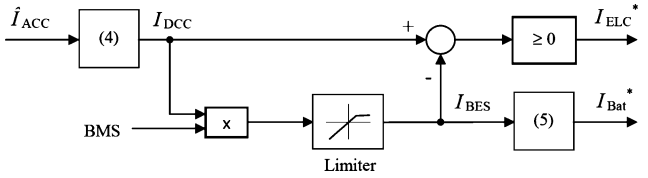

Fig. 4. Reference current distribution to dc–dc converter controllers.

power is supplied by means of the electronic converter and the capacitor bank. The ac voltage regulator determines the aforementioned current reference (i_{Cq}) that, consequently, is in quadrature with the sensed three-phase voltage signals.

The voltage imbalance in the dc bus capacitors (due to ac load and device asymmetries in the power converter) is corrected by a current control loop and a voltage-control loop [13]. The reference signal i^*_{CNN} is determined from measured three-phase load currents and voltage difference between capacitor C_1 and C_2 (3)

$$\begin{aligned} i^*_{\mathrm{CNN}} &= -(i_{\mathrm{L\,n}} + k\, v_{\mathrm{dif}}) \\ &= (i_{\mathrm{L\,a}} + i_{\mathrm{L\,b}} + i_{\mathrm{L\,c}}) - k\,(v_{\mathrm{C1}} - v_{\mathrm{C2}}). \end{aligned} \tag{3}$$

Finally, the three-phase and neutral currents of converter are controlled by using a hysteretic controller for each branch. Each controller acts over the corresponding difference between the reference currents of the converter $i_{\mathrm{C}}(\mathrm{a,b,c,n})^*$ and the measured ac-side currents i_{C} (a,b,c,n). The hysteretic controller gives the IGBT gating signals ($\mathrm{S_A}$ to $\mathrm{S_D}$) of the four-leg VSC.

B. Current Control of the DC–DC Converters

The frequency regulator determines the complementary ac current magnitude ($\hat{I}_{\mathrm{ACC}}$). This magnitude yields an active power value that is equivalent to dc power. It is divided by the voltage value on the dc bus V_{DC}, thus generating the reference current I_{DCC} for dc–dc converters (Fig. 4)

$$I_{\mathrm{DCC}} = \frac{3V_{\mathrm{S}}}{\sqrt{2}V_{\mathrm{DC}}}\hat{I}_{\mathrm{ACC}}. \tag{4}$$

Then, the component I_{DCC} is the sum of the reference signals to the electronic load controller (I_{ELC}) and BES system (I_{BES}). The distribution of both currents is carried out by a limiter block. A last block (5) computes the suitable value of battery current according to the voltage ratio between the dc bus and battery bank

$$I_{\mathrm{Bat}} = \frac{V_{\mathrm{DC}}}{V_{\mathrm{Bat}}} I_{\mathrm{BES}}. \tag{5}$$

When the SEIG is working without the ac load, the reference I_{DCC} includes the battery current value (let us suppose, for example, limited to 60% of the SEIG rated current) and the reference to the controlled dc load (corresponding to the remaining excess active power).

However, when an ac load is switched on to the SEIG, the demand of generating power is increased; this yields a reduction in the rotor speed and, consequently, of the frequency value. So, the lower output signal of the frequency regulator forces the reduction of the current through the dc–dc converters. First, it decreases the current corresponding to the power dissipated by the chopper, and the battery keeps its value of charge current. But if this behavior is not enough, the bidirectional converter decreases the battery charge current to a suitable value. If the ac load is higher, then this last converter forces the battery to inject a determinate value of current to the ac side of the system, through to the VSI.

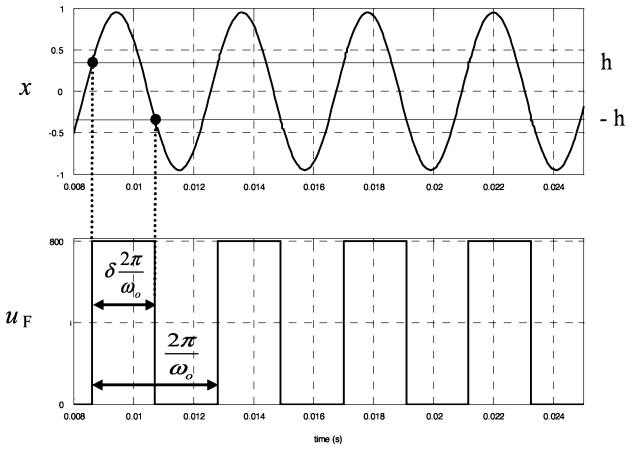

Fig. 5. Waveforms of the self-oscillating relay system.

Finally, in the proposed control scheme, there is a binary input called battery state (BS). The value of this signal is determined by the battery-management system. This specific unit places the signal at 0 BS if some problem exists (i.e., temperature ...) or the battery is charged. So the battery converter is disabled, and the resistive dc load must absorb the whole magnitude of I_{DCC} (if it is positive).

1) BES System: The current controller of the bidirectional dc–dc converter is based in a relay with hysteresis ($\pm$h). This is a relay system with asymmetrical output: $u_{\mathrm{F}} = +\mathrm{V_{DC}}$ or 0 V (Fig. 5).

The existence of a limit cycle in a relay feedback system is determined by the hysteresis of the comparator unit and the transfer function of the linear plant. This situation involves the relay system oscillating with a certain frequency ω_o and duty cycle δ.

The periodic sequence of pulses $u_{\mathrm{F}}(t)$ can be expressed by means of a Fourier series as a sum of harmonic components

$$u_{\mathrm{F}}(t) = \delta V_{\mathrm{DC}} + \frac{2V_{\mathrm{DC}}}{\pi}\sum_{n=1}^{\infty}\frac{1}{n}\sin(n\delta\pi)\cos(n\omega_o t). \tag{6}$$

A necessary condition of stability in a relay feedback system [14] is that the relative degree of the transfer function of its linear part should not exceed two and that all of the roots (poles and zeros) must be located in the left-half s-plane [15].

In this case, since the relative degree of transfer function (1) of the LCL filter is 3, the relay control system would be unstable. To compensate this system and, thus, reach a limit cycle, we propose reducing the relative degree of its linear part by means of a parallel stage (Fig. 6); with a first-order transfer function (7)

$$C_p(s) = \frac{\mathrm{K_C}}{\mathrm{L_C}s + \mathrm{R_C}}. \tag{7}$$

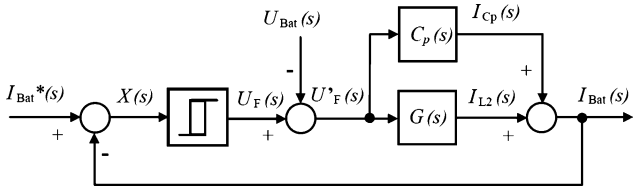

Fig. 6. Block diagram of the relay system with compensator.

As a result, after the compensation, the modified LCL filter is a system with relative degree one

$$Gc(s) = \frac{B_3 s^3 + B_2 s^2 + B_1 s + B_0}{A_4 s^4 + A_3 s^3 + A_2 s^2 + A_1 s + A_0} \tag{8}$$

where

$$\begin{aligned}
B_3 &= \mathrm{K_C L_1 L_2 C_3};\\
B_2 &= \mathrm{K_C(R_{L2} L_1 C_3 + R_{L1} L_2 C_3)};\\
B_1 &= \mathrm{K_C(R_{L1} R_{L2} C_3 + L_1 + L_2) + L_C};\\
B_0 &= \mathrm{K_C(R_{L1} + R_{L2}) + R_C};\\
A_4 &= \mathrm{L_1 L_2 L_C C_3};\\
A_3 &= \mathrm{C_3(R_{L1} L_2 L_C + R_{L2} L_1 L_C + R_C L_1 L_2)};\\
A_2 &= \mathrm{C_3(R_{L1} R_{L2} L_C + R_{L1} R_C L_2 + R_{L2} R_C L_1) + L_C(L_1 + L_2)};\\
A_1 &= \mathrm{R_{L1} R_{L2} R_C C_3 + L_C(R_{L1} + R_{L2}) + R_C(L_1 + L_2)};\\
A_0 &= \mathrm{R_C(R_{L1} + R_{L2})}.
\end{aligned}$$

For $\mathrm{K_C} = 1$ and taking $\mathrm{L_C}$ and $\mathrm{R_C}$ values from 2 to 20 times the reference values of $\mathrm{L_1}$ and $\mathrm{R_{L1}}$, we can determine that all poles and zeros of transfer function $G_C(s)$ are in the left s half-plane. Thus, in this range of parameter, $G_C(s)$ is a minimum phase system. This condition guarantees the system stability for small perturbations.

According to (6) and (8), the battery current is determined by (9). This expression has a constant term and a periodic term. $|G_{\mathrm{C}}(0)|$ is the magnitude of the compensated LCL filter frequency response for a dc component input

$$\begin{aligned}
\tilde{i}_{\mathrm{Bat}}(t) &= i_{\mathrm{Bat}\,0} + \tilde{i}_{\mathrm{Bat}\,1}(t)\\
&= \left(\frac{\mathrm{V_{DC}}}{2} - V_{\mathrm{Bat}}\right)|Gc(0)| + \frac{\mathrm{V_{DC}}}{2}(2\delta - 1)|Gc(0)|\\
&\quad + \frac{2\mathrm{V_{DC}}}{\pi}\sum_{n=1}^{\infty}\frac{|Gc(n\omega_o)|}{n}\\
&\quad \times \sin(n\delta\pi)\cos(n\omega_o t - n\delta\pi + \theta(n\omega_o)).
\end{aligned} \tag{9}$$

The variation of the battery current reference signal (i^*_{Bat}) is comparatively slow with respect to the periodic term of battery current. So that input reference may be considered constant during the period $2\pi/\omega_o$. From [15] and according to Fig. 5, the conditions for the existence of self-oscillations in this dc–dc converter are given by

$$\begin{aligned}
\tilde{x}\left(\delta\frac{2\pi}{\omega_o}\right) &= -h = I^*_{\mathrm{Bat}} - \left(\frac{\mathrm{V_{DC}}}{2} - V_{\mathrm{Bat}}\right)\\
&\quad \times |Gc(0)| - \tilde{i}_{\mathrm{Bat1}}\left(\delta\frac{2\pi}{\omega_o}\right)\\
\tilde{x}\left(\frac{2\pi}{\omega_o}\right) &= h = I^*_{\mathrm{Bat}} - \left(\frac{\mathrm{V_{DC}}}{2} - V_{\mathrm{Bat}}\right)\\
&\quad \times |Gc(0)| - \tilde{i}_{\mathrm{Bat1}}\left(\frac{2\pi}{\omega_o}\right)\\
\dot{\tilde{x}}^-\left(\delta\frac{2\pi}{\omega_o}\right) &< 0, \quad \dot{\tilde{x}}^-\left(\frac{2\pi}{\omega_o}\right) > 0.
\end{aligned} \tag{10}$$

The value of ω_o and δ can be obtained by a frequency-domain method consisting of plotting the Tsypkin locus defined as (11)

$$\begin{aligned}
T_1(\omega) &= -\frac{1}{\omega}\dot{\tilde{i}}^-_{\mathrm{Bat}\,1}\left(\frac{2\pi}{\omega}\right) - j\tilde{i}_{\mathrm{Bat}\,1}\left(\frac{2\pi}{\omega}\right)\\
T_\delta(\omega) &= -\frac{1}{\omega}\dot{\tilde{i}}^-_{\mathrm{Bat}\,1}\left(\delta\frac{2\pi}{\omega}\right) - j\tilde{i}_{\mathrm{Bat}\,1}\left(\delta\frac{2\pi}{\omega}\right).
\end{aligned} \tag{11}$$

Finally, with the time derivative of (9) and applying the appropriate simplifications, the expressions of Tsypkin locus are

$$\begin{aligned}
T_1(\omega) &= -\frac{\mathrm{V_{DC}}}{\pi}\left[\sum_{n=1}^{\infty}[(1-\cos(2n\delta\pi))\Re(Gc(n\omega))\right.\\
&\quad \left. - \sin(2n\delta\pi)\Im(Gc(n\omega))] - \frac{\pi\mathrm{K_C}}{2\omega\mathrm{L_C}}\right]\\
&\quad - j\frac{\mathrm{V_{DC}}}{2}\left[(2\delta-1)|Gc(0)|\right.\\
&\quad + \frac{2}{\pi}\sum_{n=1}^{\infty}\left[\frac{\sin(2n\delta\pi)}{n}\Re(Gc(n\omega))\right.\\
&\quad \left.\left. + \frac{1-\cos(2n\delta\pi)}{n}\Im(Gc(n\omega))\right]\right]\\
T_\delta(\omega) &= -\frac{\mathrm{V_{DC}}}{\pi}\left[\sum_{n=1}^{\infty}[-(1-\cos(2n\delta\pi))\Re(Gc(n\omega))\right.\\
&\quad \left. - \sin(2n\delta\pi)\Im(Gc(n\omega))] + \frac{\pi\mathrm{K_C}}{2\omega\mathrm{L_C}}\right]\\
&\quad - j\frac{\mathrm{V_{DC}}}{2}\left[(2\delta-1)|Gc(0)|\right.\\
&\quad + \frac{2}{\pi}\sum_{n=1}^{\infty}\left[\frac{\sin(2n\delta\pi)}{n}\Re(Gc(n\omega))\right.\\
&\quad \left.\left. - \frac{1-\cos(2n\delta\pi)}{n}\Im(Gc(n\omega))\right]\right].
\end{aligned} \tag{12}$$

The Tsypkin function is an infinite series. However, the convergence of this series is determined by the transfer function $G_C(s)$. As a result, only the sum of a few first terms of (12) is enough to calculate the value for each frequency.

According to (10) and (12), the limit cycle exists if the Tsypkin locus intersects the respective straight line given by

$$\begin{aligned}
&\Im[r_1] = -I^*_{\mathrm{Bat}} + h + \left(\frac{\mathrm{V_{DC}}}{2} - V_{\mathrm{Bat}}\right)|Gc(0)|,\\
&\Re[r_1] > 0\\
&\Im[r_\delta] = -I^*_{\mathrm{Bat}} - h + \left(\frac{\mathrm{V_{DC}}}{2} - V_{\mathrm{Bat}}\right)|Gc(0)|,
\end{aligned}$$

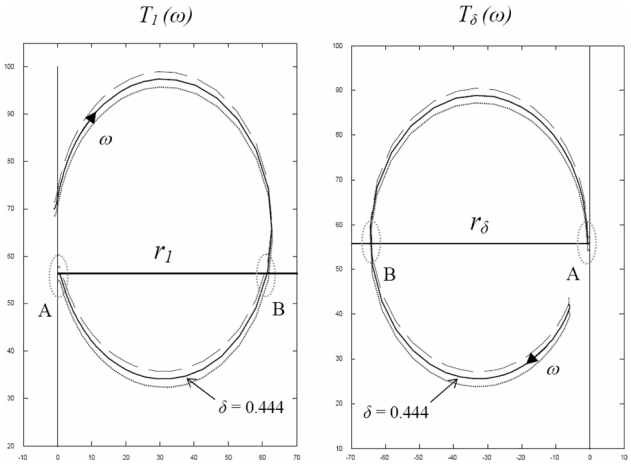

Fig. 7. Family of Tsypkin locus $T_1(\omega) - T_\delta(\omega)$ and its intersections between the straight lines $r_1 - r_\delta$.

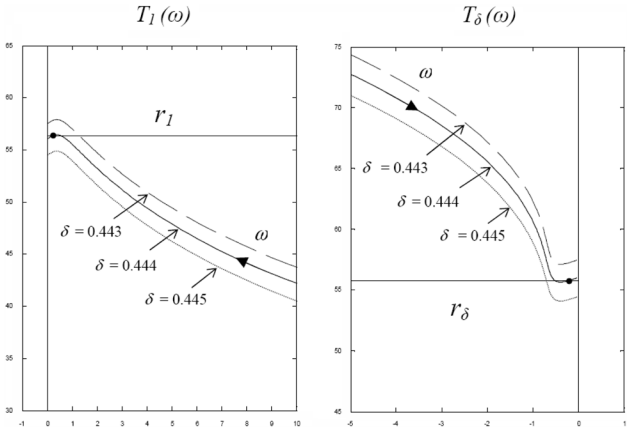

Fig. 8. Detail of the intersection point between the high-frequency Tsypkin locus and respective straight line (zone A).

$$\Re[r_\delta] < 0. \tag{13}$$

In this case, for a reference signal $(I_{\mathrm{Bat}})^*)$ equal to 7 A, consider $(\mathrm{L_C}, \mathrm{R_C}) = 3.5(\mathrm{L_1}, \mathrm{R_{L1}})$ and $\mathrm{h} = 0.3$, the result that the intersection points between the respective Tsypkin locus and straight-line yields two possible zones: A and B (Fig. 7). The first area determines a stable limit cycle with $f_o = 17.2$ kHz and $\delta = 0.444$ (Fig. 8). The option B returns a limit cycle with $f_o = 3.3$ kHz and high amplitude oscillations ($\pm$ 50 A)

Finally, under the constraint of no plant leakage configurations [16], the parallel compensator $C(s)$ is replaced by a feedback unit connected across the relay element (Fig. 9).

The practical relay feedback control has a proportional-integral (PI) regulator to compensate steady-state error between the reference and the battery current.

2) Electronic Load Controller: The controller of this second dc–dc converter subtracts the reference signal $\mathrm{I^*_{ELC}}$ (current distribution block, Fig. 4) from the mean value of sensed current in $\mathrm{R_{DC}}$. This current error is applied to a PI controller and then is compared with a triangular carrier wave to generate the PWM signal $(\mathrm{S_E})$ for switching the respective IGBT. The selected frequency for this triangular wave is 10 kHz.

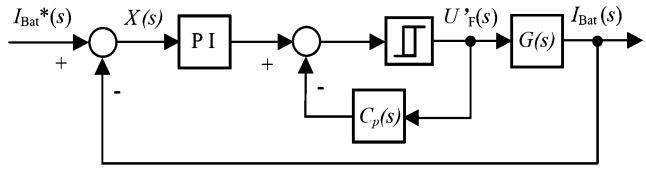

Fig. 9. Block diagram of definitive relay control system.

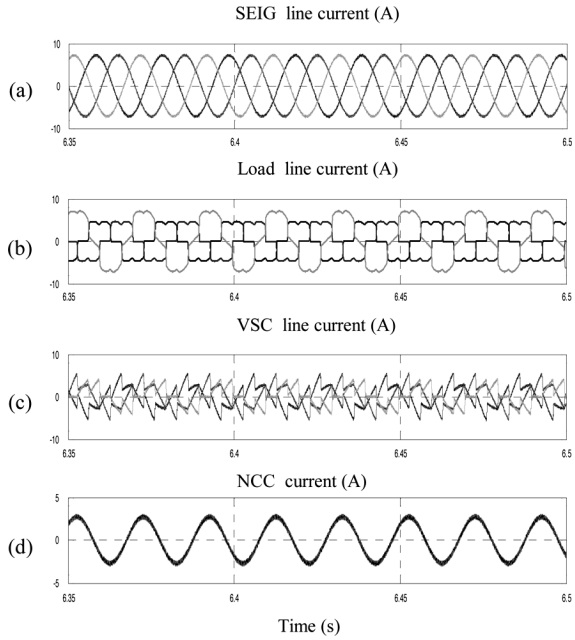

Fig. 10. Current waveforms on the ac side of the system for three-phase four-wire unbalanced and nonlinear load conditions.

The proposed control architecture allows the compound converter to eliminate current harmonics, to compensate the reactive power, and to balance the load current at the SEIG terminals, as well as to store or inject the suitable value of power depending on the ac load needs. So the whole system increases its efficiency and capability

IV. Simulation Results

This section shows the system performance by means of some simulation results. The proposed system was modeled and simulated in MATLAB, with Simulink and SimPowerSystems toolboxes. The simulation is carried out with the ode23tb (stiff/TR-BDF2) solver. The system parameters are given in the Appendix.

Fig. 10 shows the steady-state current waveforms on the ac side of the system for unbalanced and nonlinear three-phase four-wire load conditions. More specifically, the load set is made up of a single-phase resistive load ($(\mathrm{R} = 120\ \Omega/\mathrm{V_{ph}} = 230$ V) and a three-phase rectifier bridge connected to a resistive dc load $(\mathrm{R} = 120\ \Omega)$ with shunt capacitor $(\mathrm{C} = 100\ \mu\mathrm{F})$. So the current magnitude of each phase in this load set is distorted and not equal (b), but means that the action of the four-leg VSC (c) and the SEIG (d) supplies a balanced current with sinusoidal waveforms (a).

The two figures below illustrate the system dynamic response for different load conditions and rotor speed. First, SEIG works

without the ac load, so the dc-dc converters consume all of the generated power. Most active power flows to the battery converter and chopper, only a small amount of this active power keeps the voltage level in the dc bus of this converter. At this operating point, the switching frequency of the bidirectional dc–dc converter is 17.5 kHz, the battery current is 7 A, and ripple current is ±50 mA. These values correspond to the limit cycle zone A obtained by the Tsypkin method.

Fig. 11 shows the transient response on the SEIG and electronic converter when a set of balanced three-phase loads is switched (b). First, a three-phase load of 2 kW is connected to the ac supply system. Then, at 4.75 s, an inductive three-phase load $(\mathrm{S} = 2\ \mathrm{kVA/PF} = 0.85)$ is applied and, finally, at 5.3 s, the first load is disconnected from the ac induction generator. This action implies heavy variations in the ac and dc magnitudes of the converter. However, the controller responds by driving (c) the magnitude (d) and frequency of the generated voltage to their reference values. The current through (e) VSC and (f) dc–dc converters (f) flows as a function of the ac load conditions. At the beginning, the current decreases in the ELC unit (dashed line) and then, the battery stores or injects a suitable value of current (solid line) by means of the controlled bidirectional battery converter. This characteristic allows increasing the efficiency and availability of the proposed generating system.

Fig. 12 shows the performance of this autonomous system when the induction generator is feeding a three-phase balanced inductive load $(\mathrm{S} = 2\ \mathrm{kVA/PF} = 0.85)$ and (b) the prime mover reduces the rotor speed from 1547 r/min to 1520 r/min. In this situation, (a) the SEIG current decreases, the resistive dc load is disabled, and (f) the battery supplies the suitable current value through (e) the VSC , to reach (c) the rated phase voltage and (d) frequency in the three-phase system.

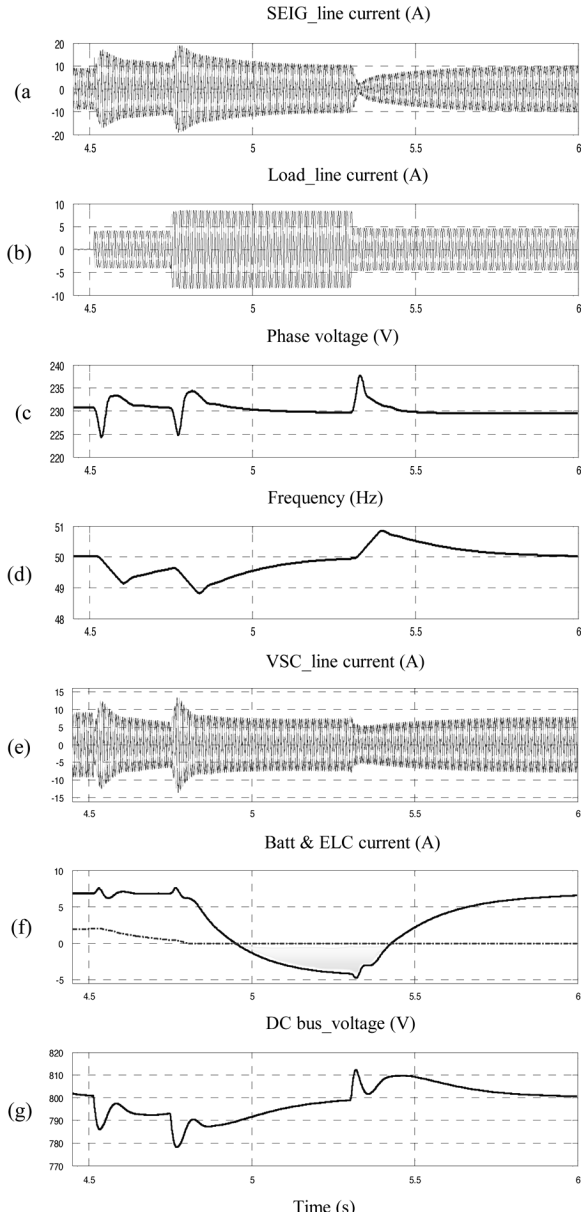

Fig. 11. Transient behavior of the system under different balanced load conditions.

V. Conclusion

This paper has presented a controller's architecture for an SEIG-STATCOM system operating in collaboration with a controlled dc load and a BES system. The Tsypkin method is applied to analyze the self-oscillating bidirectional dc–dc converter associated with the battery bank.

The proposed converter and its control loops allow attenuating current harmonics, compensating reactive power, and balancing the SEIG currents, while the energy storage system can store or inject active power and, if necessary, the controlled dc load dissipates the remaining generated power. So the SEIG maintains the rated voltage and frequency under different loading conditions, moreover, increasing the efficiency and availability of the system. Finally, the simulation results show good performance and power-quality improvement of the whole system under different loading conditions and variable rotor speed.

Appendix

The corresponding system parameters used to obtain the simulation results are:

- Three-phase induction machine and shunt capacitor
  $P = 4$ kW, $\mathrm{V_{AC}} = 400$ V (Y), $\mathrm{f} = 50$ Hz, 4 poles,
  $\mathrm{R_s} = 1.365\ \Omega, \mathrm{R_r} = 1.405\ \Omega, \mathrm{L_{ls}} = \mathrm{L_{lr}} = 5.839$ mH,
  $\mathrm{L_m} = 0.083I_{\mathrm{m}}^5 - 2.2I_{\mathrm{m}}^4 + 21.4I_{\mathrm{m}}^3 - 89.3I_{\mathrm{m}}^2 + 124I_{\mathrm{m}} + 205$ [mH], where I_{m} is the magnetizing current (in amperes)
  $\mathrm{C_{AC}} = 3 \times 90\ \mu$ F, Y connected.
- Electronic converter $\mathrm{R_{DC}}$ and battery
  $\mathrm{C_1} = \mathrm{C_2} = 3000\ \mu$F, $\mathrm{C_3} = 4.7\ \mu$F,
  $\mathrm{L_{ph}} = \mathrm{L_N} = 10$ mH, $\mathrm{R_{Lph}} = \mathrm{R_{LN}} = 0.8\ \Omega$,
  $\mathrm{L_1} = 4.7$ mH, $\mathrm{R_{L1}} = 0.5\ \Omega, \mathrm{L_2} = 0.6$ mH, $\mathrm{R_{L2}} = 0.1\ \Omega$,
  $\mathrm{R_{DC}} = 300\ \Omega$, $\mathrm{V_{Bat}} = 350$ V, $\mathrm{R_{Bat}} = 0.75\ \Omega$.
- PI controllers
  $\mathrm{V_{AC}} : \mathrm{K_P} = 0.3, \mathrm{K_I} = 0.5$; $\mathrm{V_{DC}} : \mathrm{K_P} = 0.1, \mathrm{K_I} = 1.25$
  Freq: $\mathrm{K_P} = 1.2, \mathrm{K_I} = 40$; PLL : $\mathrm{K_P} = 50, \mathrm{K_I} = 5$
  $\mathrm{I_{ELC}} : \mathrm{K_P} = 1, \mathrm{K_I} = 300$; $\mathrm{I_{Bat}} : \mathrm{K_P} = 1.25, \mathrm{K_I} = 150$.

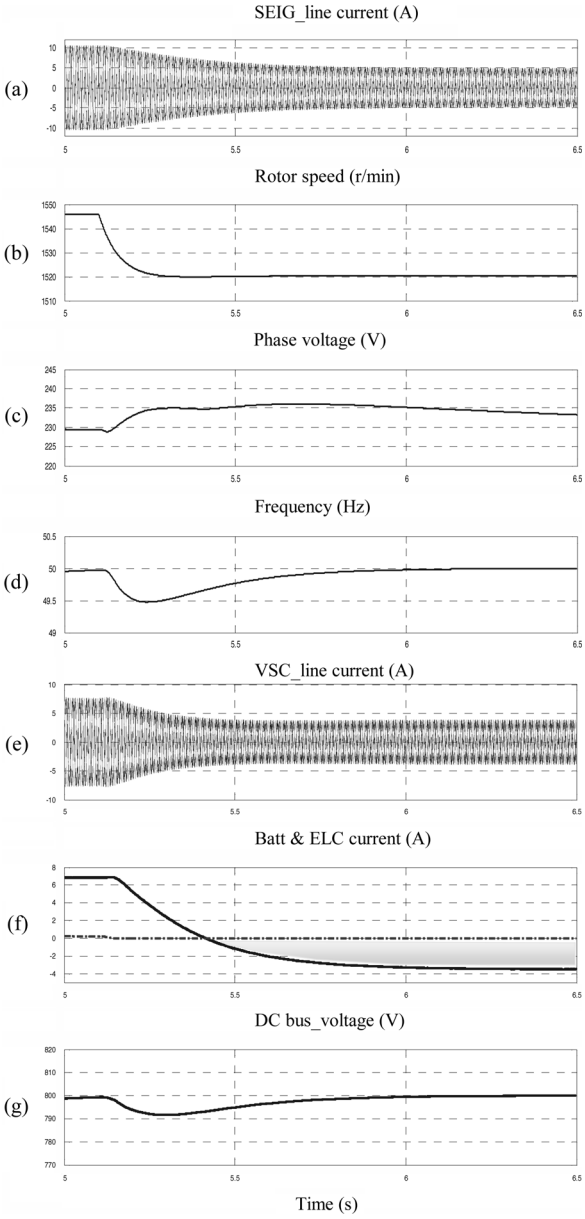

Fig. 12. Dynamic response of the system under rotor speed reduction.

REFERENCES

[1] M. Godoy and F. A. Farret, *Renewable Energy Systems. Design and Analysis With Induction Generators*. Boca Raton, FL: CRC, 2004.

[2] B. Singh and G. K. Kasal, "Analysis and design of voltage and frequency controllers for isolated asynchronous generators in constant power applications," in *Proc. Int. Conf. Power Electronics, Drives and Energy Systems*, Dec. 12–15, 2006, pp. 1–7.

[3] J. A. Barrado, R. Griñó, and H. Valderrama, "Standalone self-excited induction generator with a three-phase four-wire active filter and energy storage system," in *Proc. IEEE Int. Symp. Industrial Electronics*, Jun. 4–7, 2007, pp. 600–605.

[4] L. Martínez-Salamero, H. Valderrama-Blavi, and R. Giral, "Self-oscillating DC-DC switching converters with transformer characteristics," *IEEE Trans. Aerosp. Electron. Syst.*, vol. 41, no. 2, pp. 710–716, Apr. 2005.

[5] D. R. Williams, C. Bingham, D. A. Stone, M. P. Foster, and A. Gilbert, "Analysis of self-oscillating DC-DC resonant power converters using a hysteretic relay," in *Proc. Eur. Conf. Power Electronic and Applications*, Sep. 2–5, 2007, pp. 1–9.

[6] Y. Hu, J. Tatler, and Z. Chen, "A bi-directional DC-DC power electronic converter for an energy storage device in an autonomous power system," in *Proc. Int. Power Electronics and Motion Control Conf.*, Aug. 14–16, 2004, vol. 1, pp. 171–176.

[7] P. Rodriguez, R. Pindado, and J. Bergas, "Alternative topology for three-phase four-wire PWM converters applied to a shunt active power filter," in *Proc. IEEE Annu. Conf. Industrial Electronics Soc.*, Nov. 5–8, 2002, vol. 4, pp. 2939–2944.

[8] B. Singh, A. Chandra, G. K. Kasal, and K. A. Haddad, "A frequency based electronic load controller for an isolated asynchronous generator feeding 3-phase 4-wire loads," in *Proc. IEEE Int. Symp. Industrial Electronics*, Jun. 30–Jul. 2, 2008, pp. 1513–1518.

[9] M. Bojrup, "Advanced control of active filters in a battery charger application," Licentiate thesis, Lund University, Lund, Sweden, 1999.

[10] Q. Wang and S. S. Choi, "The design of battery energy storage system in a unified power-flow control scheme," *IEEE Trans. Power Del.*, vol. 23, no. 2, pp. 1015–1024, Apr. 2008.

[11] M. Karimi-Ghartemani and M. R. Iravani, "A method for synchronization of power electronic converters in polluted and variable frequency environments," *IEEE Trans. Power Syst.*, vol. 19, no. 3, pp. 1263–1270, Aug. 2004.

[12] P. Rodriguez, R. Pindado, and J. Pou, "Energy control of three-phase four-wire shunt active power filter," in *Proc. IEEE Annu. Conf. Industrial Electronics Society*, Nov. 2–6, 2003, vol. 2, pp. 1061–1066.

[13] M. M. Mishra, A. Joshi, and A. Ghosh, "Control schemes for equalization of capacitor voltages in neutral clamped shunt compensator," *IEEE Trans. Power Del.*, vol. 18, no. 2, pp. 538–544, Apr. 2003.

[14] J. M. Gonçalves, A. Megretski, and M. A. Dahleh, "Global stability of relay feedback systems," *IEEE Trans. Autom.Control*, vol. 46, no. 4, pp. 550–562, Apr. 2001.

[15] Y. Z. Tsypkin, *Relay Control Systems*. Cambridge, U.K.: Cambridge Univ.Press, 1984.

[16] C.-T. Chen, "Introduction to the linear Algebraic method for control system design," *IEEE Control Syst. Mag.*, vol. 7, no. 5, pp. 36–42, Oct. 1987.

J. A. Barrado received the electronic engineering degree from the Universitat de Barcelona (UB), Spain, in 2000 and the Ph.D. degree in automatic control from Universitat Politècnica de Catalunya, Barcelona, Spain, in 2008.

He is currently an Assistant Professor with the Department of Electronic Engineering and Automatic Control of the Universitat Rovira i Virgili, Tarragona, Spain. His research interests include analysis, modeling and control of electrical generators, and power converters applied to renewable energy systems.

R. Griñó (S'90–M'99) received the M.Sc. degree in electrical engineering and the Ph.D. degree in automatic control from the Universitat Politècnica de Catalunya (UPC), Barcelona, Spain, in 1989 and 1997, respectively.

From 1990 and 1991, he was a Research Assistant with the Instituto de Cibernética, UPC. From 1992 to 1998, he was an Assistant Professor with the Department of Systems Engineering and Automatic Control and the Institute of Industrial and Control Engineering, UPC, where he has been an Associate Professor since 1998. His research interests include digital control, nonlinear control, and control of power-electronic converters.

H. Valderrama-Blavi (M'04) received the ingeniero de telecomunicación degree and the Ph.D. degree from the Universitat Politècnica de Catalunya (UPC), Barcelona, Spain, in 1994 and 2001, respectively.

He is currently an Associate Professor with the Department of Electronic Engineering and Automatic Control of the Universitat Rovira i Virgili, Tarragona, Spain, where he is working in the field of inverters for photovoltaic systems, wind systems, fuel cells, and grid-tie systems.